EVALUATION OF RADARSAT-SAR DATA FOR DETECTION OF TERRAIN FEATURES

R.S.Dwivedi, P.Sathyanarayana, Ch.Venkateswara Rao, A.S.Manjunath
National Remote Sensing Agency
(Dept.of Space, Govt.of India)
Balanagar, Hyderabad-500 037.

KEYWORDS: Synergism, Radarsat-SAR, Optical sensor, Cloud-penetration,Terrain features, Speckle suppression, Salt-affected soils

ABSTRACT

The spaceborne multispectral optical sensor data have been routinely used for assessment and monitoring of natural resources and environment. One of the major problems associated with the optical data is the availability of cloud-free data during rainy season Cloud-penetration capability of microwave sensors data offers immense potential in the study of highly dynamic phenomenon like floods. We have taken up this study to evaluate the potential of Radarsat fine beam mode SAR data for detection of various terrain features; and to study the complementarity of this data with the optical sensors data from the Indian Remote Sensing Satellite (IRS-1C) Linear Imaging Self-scanning Sensor (LISS-III) and Panchromatic sensor (PAN) over parts of Haryana state, India. The approach essentially involves speckle suppression, digital image registration, extraction of common areas; intensity, hue and saturation (IHS) transformation for merging SAR data with the optical sensor data and subsequent evaluation of these data sets for detection of terrain features. The results indicate a good synergy of the SAR data with the optical sensor data in providing information on various terrain features. The methodology and results are discussed in detail.

1. INTRODUCTION

The spaceborne multispectral data have been operationally used for mapping and monitoring natural resources-both renewable and non-renewable since the launch of ERTS-1 (later renamed as Landsat) in the early 1970s. One of the major problems associated with the availability of good quality spaceborne optical data is the presence of thick and widespread cloud cover during monsoon season (rainy season) which precludes generation of timely information on various natural resources and environment especially on crops and floods. Synthetic Aperture Radar (SAR) sensors offer additional advantages of an all-weather, day or night data collection capability as well as synergistic studies with the optical data. There are several civilian satellites in space for microwave imaging including ERS-1 and 2, JERS-1 and Radarsat. Radarsat offers a flexible system configuration which enhances data coverage and application potential.

SAR data have been successfully used for mapping geological features/structures covered with sand overburden (Schaber et al. 1997) , detection of palaeodrainage (Dabbagh et al. 1997), and volcanic mapping (Huadong et al. 1997). Soil moisture estimation (Dobson and Ulaby, 1986; Wang et al. 1997), flood mapping (Pope et al. 1997), snow mapping (Shi and Dozier, 1997) and observation of rainstorm and rain measurement (Jameson et al. 1997 and Moore et al. 1997) are other applications where SAR data has provided encouraging results. In addition, crop discrimination (Soares et al. 1997) and crop monitoring (Brisco et al. 1995) have been achieved using SAR data. Further, forest categorization and estimation of biomass density (Ranson and Sun, 1997), deforestation (Ringot et al. 1997) and biomass estimation (Harrel et al. 1997) are other promising areas of SAR applications. Considering the vast potential of SAR data in various applications, as mentioned earlier, the study aims at evaluating the potential of Radarsat-SAR data vis-a-vis ERS-1 SAR data for detection of various terrain features, and at studying the synergism of SAR data with the optical data from IRS-1C LISS-III and PAN sensors in part of Haryana state, India.

2. THE STUDY AREA

Bound between geo-coordinates 29° 20' to 29° 50' N and 75° 45' to 76° 50' E, the study area forms parts of Karnal, Jind and Hisar districts of Haryana state (Figure-1). Four test site each covering about 2.5kmX2.5km around Sherah (Karnal district), Kakrod and Badanpur (Jind district) and Tohana (Hisar district) have been selected for intensive study. Physiographically, it is part of the vast Indo-Gangetic alluvial plain which is dotted with the palaeochannels and is covered at places with the aeolian material. Most of the area is under a variety of crops and there is a very good canal network. The area experiences a sub-tropical, continental, monsoonal and semi-arid climate with the mean annual precipitation ranging from 353.0mm (Hisar) to 521mm (Jind).

3. THE DATA USED

Radarsat-SAR digital data acquired in the fine beam (F5) mode with 6.25m spatial resolution covering the test sites were used as primary data (Table-1). In addition, we have also used archived ERS-1 SAR data closer to Radarsat data acquisition period. Further, IRS-1C PAN and LISS-III data have been used to study the synergism between these data and SAR data. Survey of India topographical sheets at 1:50,000 and 1:250,000 scale were used as ancillary data.

4. METHODOLOGY

4.1 Speckle Suppression :

Owing to coherent nature of SAR data, it is difficult to successfully adapt statistical pattern recognition methods for use on this data. The presence of speckle in SAR images often precludes a pixel-by-pixel classification unless these data have been smoothed. Various speckle suppression filters, namely simple average (Lowry et al. 1978) or median filters (Brisco and Protz, 1982), non-linear isotropic filtering (Holmes et al. 1984), Lee filter (Lee, 1981), Sigma filter (Lee 1983, 1986), Weighting filter (Martin and Turner, 1993), Li's method (Li 1988) and Maximum A Posteriori (MAP) filter (Lopes et al. 1993) have been commonly used. We have used 3x3 Frost filter, Lee filter, median filter, Gamma MAP filter and Lee-Sigma filter in a Silicon Graphics workstation with ERDAS - Imagine version 8.3 software.

4.2 Image Registration :

The next logical step was the digital image registration of Radarsat-SAR data with other data, namely ERS-1 SAR and IRS-1C PAN and LISS-III data. It was achieved by taking Radarsat-SAR data as a reference and registering the IRS-1C PAN data to a subpixel accuracy using adequate ground control points (GCPs) image-to-image tie down algorithm and second order polynomial transform. Rest of the data sets were similarly registered to Radarsat-SAR data using image-to-image tie down algorithm. Subsequently ERS-1 SAR, and IRS-1C LISS-III and PAN data were resampled to 6.25m x 6.25m pixel dimension and a common window of 400 pixels X 400 scan lines for each site was selected for further analysis.

4.3 Image Fusion :

In order to study the synergism of SAR data with the optical data, the SAR data was merged with the multispectral LISS-III data using intensity, hue and saturation (IHS), transformation. Here, the intensity component of LISS-III data was replaced by Radarsat-SAR data after speckle suppression.

4.4 Data Evalulation :

The output images from each sensor, thus generated, were evaluated for the ease of detection of various terrain features both natural like sand dunes, salt-affected soils, waterbodies, etc; as well as cultural features, namely roads, railways, canals, bridges, settlements, field boundaries, etc. based on authors' experience and the information available in the Survey of India topographical sheets of 1:50,000 and 1:250,000 scale. In addition, we have drawn a comparison amongst various data sets with respect to detectability of various terrain features.

5. RESULTS

Initially, a brief description of various speckle suppression filters alongwith their merits will be presented. It will be followed by the detectability of various terrain features on SAR data. Ultimately, the results of the assessment of individual data set including hybrid image generated by fusion techniques, with respect to relative ease of detection of various terrain features will be presented.

5.1 Speckle Suppression :

As mentioned earlier, six speckle suppression filters, namely mean, median, Lee, Lee-Sigma, Frost and Gamma MAP with 3x3 kernel were employed on Radarsat-SAR and ERS-1 SAR data after selecting homogeneous terrain features with varying radar-return regimes. The statistical parameters, namely mean and standard deviation were computed for various filtered images. Results are given in Table-2. It is evident from the table that the Gamma MAP filter with a coefficient of variation (CV) value of 0.25 has performed better when compared with other filters used. Similarly, other filters like Lee, Lee-Sigma and Frost also gave optimal performance at a CV value of 0.25.

5.2 Detection of Terrain Features :

In order to evaluate the potential of Radarsat-SAR data for detection of various terrain features, test sites covering features like salt-affected soils, sand dunes, crop land and settlements were selected; and an effort was made to interpret these features from Radarsat-SAR and other remote sensing data. Two types of terrain features, namely natural and cultural were considered.

5.2.1 Natural Features :

Sand dunes, salt-affected soils and natural water bodies such as tanks were interpreted through visual interpretation of remote sensing data. Sand dunes with sparse vegetation cover exhibit medium gray tone and smooth texture (Figure-2a) in the Radarsat-SAR image. This response is because of gently varying

smooth surface topography of the sand cover. Also the sand dues allow greater penetration. Sparse vegetation cover at the time of Radarsat-SAR data acquisition has limited point scatterers to a great extent, to diffusely reflect the incoming radar signal at the air-sand interface. In the red band image of LISS-III data (Figure-2b), sand dunes could be detected by their dull to bright white tone and irregular shape.

Like sand dunes, salt-affected soils too scattered back most of the incoming radar signal in the direction opposite to incident angle. Consequently, they could be seen as dark gray tone and smooth texture in the Radarsat SAR image (Figure-3a). In fact, salt-affected soils have the salt efflorescence on the surface whose grain size is generally less than 0.02 mm. As such, these particles are relatively much smaller than the wavelength of the incident radar waves. The smooth surface because of lack of vegetation gives rise to low returns. Further, except for salt resistant grasses and a few trees here and there, there are no objects which could backscatter the incident microwave energy. Salt-affected soils are not discernible in the ERS-1 SAR image. It could be attributed to coarse spatial resolution and the vertical polarization (VV) of the radar beam. Owing to low incidence angle and VV polarization even very small scatterers have also contributed to the measured backscatter from ERS-1 SAR. Salt-affected soils could be seen as white patches in the PAN data and as very light cyan colour in the LISS-III image (Figure-3b). The light cyan colour of the salt-affected soils in the LISS-III image could be due to the presence of moisture in the surface at the time of data acquisition.

Water bodies, especially tanks could be detected in the Radarsat-SAR image by their consistant dark tone due to specular reflection (Figure-3a). In the visible and near-infrared images of IRS-1C PAN and LISS-III data, water bodies are manifested as light gray to black and cyan to dark blue color, respectively (Figure-3b). However, only a few water bodies could be detected in ERS-1 SAR image. This is because the VV polarisation is quite sensitive to wind induced ripples of water surface and hence give stronger returns.

Croplands could be detected in the Radarsat-SAR image with the help of their radar signatures (Figure-4a). Croplands with the individual crop plant acting as a scatterer have imparted higher backscatter and lighter resultant tone. In the ERS-1 SAR image, croplands could be discerned with the help of ancillary data. It may probably be due to vertical polarization and low incidence angle of ERS-1 SAR sensor. Consequently, the scattering from individual plants is relatively more as compared to Radarsat-SAR which has a horizontally polarized beam (HH). Field boundaries also could be seen in the PAN image (Figure-4b).

5.2.2 **Cultural Features :**

Roads, rail tracks, canals, settlements and built-up land, field boundaries, and bridges are some of the cultural features which were interpreted from Radarsat-SAR data. Only major metalled roads especially those aligned perpendicular to radar beam could be detected in the Radarsat-SAR image (Figure-5a). Owing to coarse spatial resolution, only a few major roads are discernible in the ERS-1 SAR image. As expected, IRS-1C PAN (Figure-5b) image could bring out the maximum details on the road network followed by LISS-III image (Figure-5c) due to higher spatial resolution and spectral resolution, respectively.

Due to specific geometry of the rails, the rail tracks are expected to scatter the incoming radar beam significantly thereby making them more prominent amongst other terrain features. However, only those rail tracks aligned perpendicular to radar beam are manifested very clearly (Figure-5a) in the Radarsat-SAR image. However, those tracks aligned parallel to radar beam are also discernible with the help of collateral information. Similar is the case with the ERS-1 SAR image with respect to detectability of rail tracks. The IRS-1C PAN and LISS-III data, as expected, exhibited adequate image contrast that helped easy detection of rail tracks (Figure-5b and 5c).

The major canals and their distributaries show up quite clearly in the Radarsat-SAR image (Figure-5a). Owing to practically very low backscatter from the surface (specular reflection), the canals show up as a linear feature with very dark gray to black in the light to medium gray background. In the ERS-1 SAR image only a few major canals could be discerned. The optical sensors data, namely PAN provided the desired details on canal network. However, canal network is exhibited more explicitly in the PAN image in comparison with LISS-III images (Figure-5b and 5c).

Detection of large urban concentrations was comparatively easy in the Radarsat-SAR image owing to the high returns from the buildings and/complexes acting as corner reflectors (Figure-5a). However, only core areas with higher density of structures provided very high radar backscatter. The interspersion of cultivated lands, idle land/open spaces and scattered and almost random development of new residential areas however, precluded the delimitation of built-up lands. In the ERS-1 SAR image, only a few major settlements could be detected. Even in the optical data (PAN as well as LISS-III data) the transition areas between urban and built-up land posed the problem of their detection. Consequently, these two categories have been merged and named as urban and built-up lands.

Consequent upon consolidation of holdings, all the fields have been restructured to rectangular shape.

In the Radarsat-SAR image the alignment of one axis of the field boundaries perpendicular to radar beam has resulted in high radar 'return'. Such phenomenon is observed only in paddy lands perhaps due to corner reflection effects. As a result, the boundaries as long as more than a kilometer could be seen (Figure-4a). In the ERS-1 SAR image such feature could not be observed. The field pattern, however could be seen only in the PAN image (Figure-4b).

The bridges across canals, wherever the roads are intersecting them could be easily detected in the Radarsat-SAR image (Figure-5a). It may be attributed to the water acting as a specular back scatterer and the bridge over canal as a corner reflector, thereby providing a very high radar return. The major bridges could be discerned in the ERS-1 SAR image. Since such phenomenon does not occur in the visible and near infrared region, in the PAN and LISS-III images bridges could not be detected (Figure-5b and 5c).

5.3 **Synergism with the Optical Data** :

As pointed out earlier, the hybrid data sets from optical and SAR sensors were generated through IHS transformation. The LISS-III data was used as an input to IHS transformation and the intensity (I) was replaced in steps by Radarsat-SAR, ERS-1 SAR and PAN data. In addition, another set of FCC image with ERS-1 SAR, Radarsat-SAR and PAN data was generated by digitally overlaying these data sets. A visual comparision of Radarsat-SAR and LISS-III hybrid image reveals the following: 1) The discrimination between cotton and paddy crop is relatively better in the hybrid image as compared to LISS-III image alone. 2) Within the paddy lands, field boundaries are sharper as compared to LISS-III image. 3) The delineation of fallow lands has been easier in the hybrid image in comparision with either of the two data sets. 4) Core areas with relatively higher density of structures within the urban agglomeration are manifested very clearly in the hybrid image, and 5) The hybrid image has provided improved overall image contrast amongst various terrain features especially linear features like roads, rail tracks and canals.

By incorporating ERS-1 SAR data as one component in the IHS transformed LISS-III image, there has been an improvement in the contrast within the Narwana township. In addition, like Radarsat-SAR hybrid image, the ERS-1 SAR hybrid image has also exhibited within-the-class spectral variation in the township area. The LISS-III and PAN combination has provided the maximum terrain details. Field boundaries are, however, more clear in the Radarsat-SAR hybrid image as compared to LISS-III and PAN hybrid image.

A simple overlaying of the digitally registered images of ERS-1 SAR, Radarsat-SAR and PAN has resulted in the improved spectral contrast within the Narwana town. Besides, the sharpness of the field boundaries in paddy lands has been found to be more in this combination as compared to LISS-III and PAN hybrid image but relatively less in comparison with the Radarsat-SAR and LISS-III hybrid image.

6. CONCLUSIONS :

The study has amply demonstrated the potential of Radarsat-SAR data in the detection of various terrain features in the alluvial plains of the semi-arid region during monsoon season. Conjunctive use of SAR and optical sensor data has been found to score over individual data sets alone. Such study need to be conducted under varying terrain conditions to validate the observations. Cartosat data with 2.5m spatial resolution may further improve the utility of Radarsat-SAR fine beam mode SAR data if used conjunctively.

ACKNOWLEDGEMENTS

Authors would like to express their sincere gratitude to Dr. D.P.Rao, Director, National Remote Sensing Agency (NRSA), Hyderabad for constant encouragement and for providing necessary facilities during the course of investigation. One of the authors (Dr. R.S.Dwivedi) is also grateful to Dr. L.Venkataratnam, Group Head, Agriculture and Soils, NRSA for evincing keen interest in the study. Cartographic support from Sri. V.S.S.R.Murthy and the secretarial support from Ms. E.Jayasree are gratefully acknowledged.

REFERENCES

1. Homes, Q.A.; Nuesch, D.R. and Schuchman, R.A. 1984, Textural analysis and real-time classification of sea-ice types using digital SAR data. IEEE Transactions on Geosciences and Remote Sensing GE-22(2), pp 113-120.

2. Lowry, R.T.; Shlien, S. and Goodenough, D.G. 1978, A CCRS system for synthetic apertur radar imaging analylsis. In proceeding 5th Canadian Symposium on Remote Sensing pp 363-372.

3. Brisco B. and Protz, R. 1982, Manual and automatic crop identification with airborne radar imagery. Photogrammetric Engineering 48, pp 101-109.

4. Pope K.O., Rejmankova, E.; Paris, J.F. and Woodruff R. 1997, Detecting seasonal flooding cycles in marshes of the Yucatan peninsule with SIR-C polarimetric radar imagery. Remote Sensing of Environment 59(2), pp 157-166.

5. Ringot E; Salas, W.A. and Skole, D.L. 1997, Mapping deforestation and secondary growth in Randonia, Brazil, using imaging radar and Thematic

Mapper data. Remote Sensing of Environment. 59 (2), pp 167-179.

6. Ranson, K.J. and Sun, G. 1997, An evaluation of AIR SAR and SIR-C/X-SAR images for mapping northern forest attributes in Marine, USA. Remote Sensing of Environment 59 (2), pp 203-222.

7. Harrell, P.A.; Kasischke, E.S.; Bourgeau-Chavez, L.L.; Hanery, E.M. and Christensen Jr, N.L. 1997, Evaluation of approaches to estimating aboveground biomass in southern pine forests using SIR-C data. Remote Sensing of Environment 59(2), pp 223-233.

8. Soares, J.V., Renno, C.D.; Formapggio, A.R.; Yanasse, C.C.F. and Frery, A.C. 1997. An investigation of the selection of texture features for crop discrimination using SAR imagery. Remote Sensing of Environment. 59 (2), pp 234-247.

9. Moore, R.K.; Mogili A.; Fang, Y.; Beh, B; and Ahmad, A. 1997. Rain measurement with SIR-C/X-SAR, Remote Sensing of Environment. 59 (2), pp 280-293.

10. Shi, J. and Dozier, J. 1997, Mapping seasonal snow with SIR-C/X-SAR in mountanous areas. Remote Sensing of Environment 59(2), pp 294-307.

11. Wang, J.R.; Hsu, A.; Shi, J.C. O'Neill, P.E. and Engman, E.T. 1997. A comparison of soil moisture retrieval models using SIR-C measurements over the Little Washita river watershed. Remote Sensing of Environment. 59(2), pp 308-320.

12. Huadong, G.; Jingjuan, L.; Changlin, W., Chao, W.; Farr, T.G. and Evans, D.L. 1997, Use of multifrequency, multipolarization Shuttle Imaging Radar data for volcano mapping. Remote Sensing of Environment. 59(2), pp 364-374.

13. Schaber, G.G.; McCauley, J.F. and Breed, C.F. 1997, The use of multifrequency and polarimetric SIR-C/X-SAR data in geologic studies of Bir Safsaf, Egypt. Remote Sensing of Environment. 59(2), pp 337.

14. Dobson, M.C. and Ulaby, F.T. 1986, Preliminary evalultion of the SIR-B response to soil moisture, surface roughness and crop canopy cover. IEEE Transactions on Geosciences and Remote Sensing. GE 24(4), pp 517-526.

15. Brisco, B.; Brown, R.J.; Staples, G.; and Nazarenko, D.; 1995, Potential rice identification and monitoring with Radarsat, Proceedings, 17th Canadian Symposium on Remote Sensing. Saskatoon, Saskatchewan, June 13-15, pp 474-479.

16. Martin, F.J. and Turner, R.W. 1993. SAR speckle reduction by weighted filtering, International Journal of Remote Sensing, Vol. 14, No.9, pp. 1759-1774.

17. Lee, J. 1981. Refined filtring of image noise using local statistics, Computer Graphics Image Processing, Vol. 15, pp. 380-389.

18. Lee, J. 1983. Digital image smoothing and the sigma filter, Computer Vision, Graphics, and Image Processing, Vol. 24, pp. 255-269.

19. Lee, J. 1986. Speckle suppression and analysis for synthetic aperture radar images, Optical Engineering, Vol. 25, No.5, pp. 636-643.

20. Lee. J.S., Jurkevich, I.; Dewaele, P.; Wambacq, P.; and Oosterlinck. A.; 1994. Speckle filtering of synthetic aperture radar images: A review, Remote Sensing Review, Vol. 8, pp. 313-340.

21. Li, C. 1988. Two adaptive filters for speckle reduction in SAR images using the variance ratio, International Journal of Remote Sensing, Vol. 9, No.4, pp. 641-653.

22. Lopes, A., Nezry, E.; Touzi, R.; and Laur. H.; 1993, Structure detection and statistial adaptive filtering in SAR images, International Journal of Remote Sensing, Vol. 14, No.9, pp. 1735-1758.

23. Dabbagh, A.E.; Al-Hinai, K.G.; and Khan, M.A.; 1997, Detection of Sand-covered geologic features in the Arabian peninsula using SIR-C/X-SAR data. Remote Sensing of Environment. 59 pp 375-382.

24. Jameson, A.R.; Li, F.K.; Durden, S.L.; Haddad, Z.S.; Holt, B.; Fogarty, T.; Im, E.; and Moore, R.K. 1997, SIR-C/X-SAR observations of rainstorms. Remote Sensing of Environment. 59(2), pp 257-267.

Table-1 Details Of Remote Sensing Data Used

Sl. No.	Satellite/ Sensor	Path/Row or Orbit No.	Date of Acqui-sition	Type of Data
1.	Radarsat-SAR (Fine beam)	3873 3973	08.08.96 01.08.96	Digital
2.	ERS-1 SAR	720-189 728-189	09.01.93 07.09.94	Digital
3.	IRS-1C PAN	D4, 5 95-50 C1, 5, 7, 9	09.10.96 02.11.96	Digital
4.	IRS-1C LISS-III	95-50	15.09.96	Digital

Table-2 Relative Performance Of Various Speckle Suppression Filters

Sl. No.	Filter	Light Region Mean/ Std.Dev.	Medium Region Mean/ Std.Dev.	Bright Region Mean/ Std.Dev.
1.	Raw data	33.50 9.83	27.63 8.08	18.83 5.46
2.	Mean filter	33.65 2.75	27.88 1.28	19.95 2.62
3.	Median filter	33.72 3.05	28.43 1.45	19.53 2.02
4.	Lee filter (0.2)	33.57 6.11	27.84 4.60	19.22 3.73
5.	Lee-Sigma (0.20)	32.79 5.87	27.46 4.38	18.54 3.44
6.	Frost (0.20)	33.55 4.91	27.75 3.07	19.16 3.18
7.	Gamma MAP (0.2)	33.52 2.7	27.79 1.23	19.87 2.62

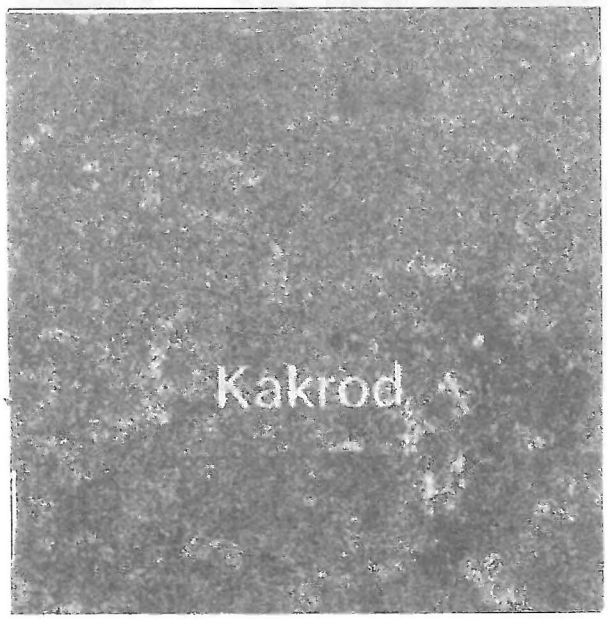

Figure-2a. Sand dunes as seen in Radarsat-SAR image of Kakrod area

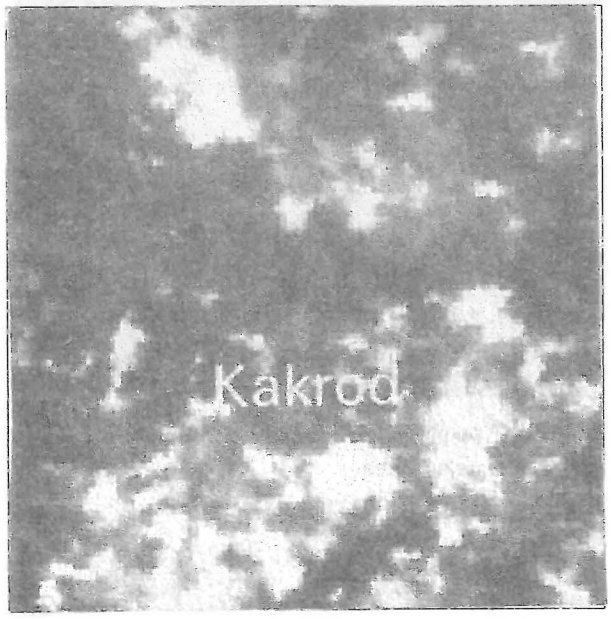

Figure-2b. Corresponding LISS-III (red band) image

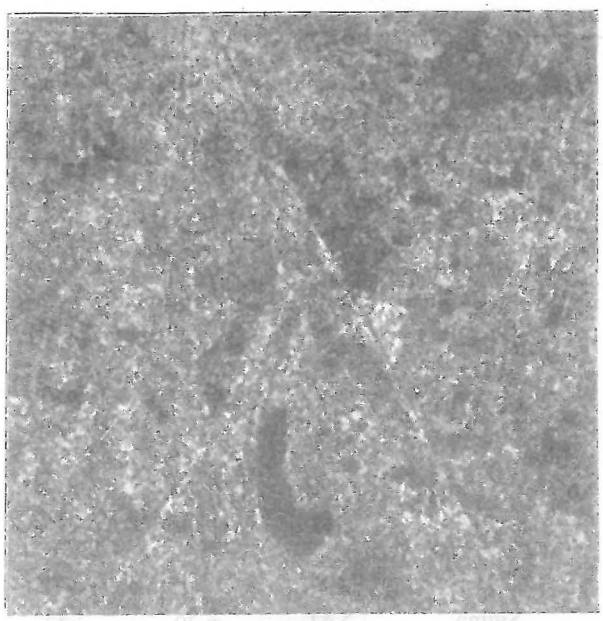

Figure-3a. Salt-affected soils as seen in Radarsat-SAR image of Sherah area

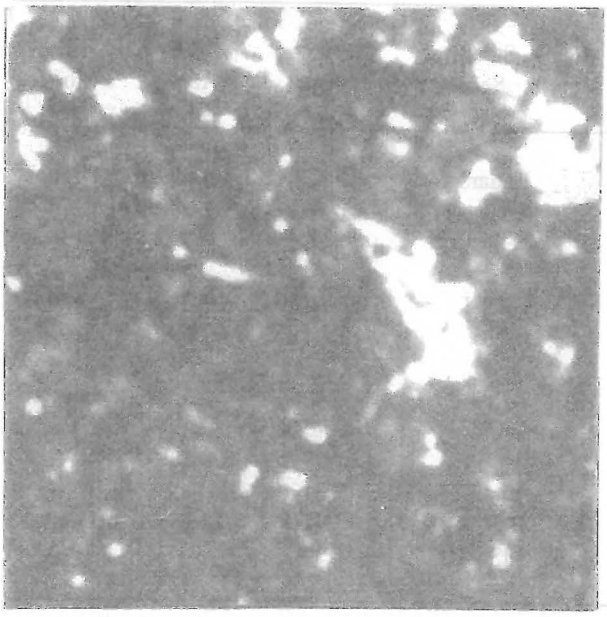

Figure-3b. Corresponding LISS-III (red band) image

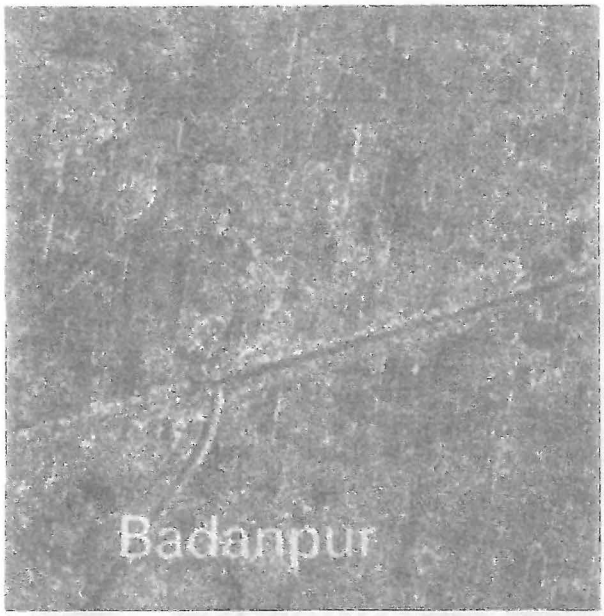

Figure-4a. Field boundaries as seen in Radarsat-SAR image of Narwana area

Figure-4b. Corresponding IRS-1C PAN image of Narwana area

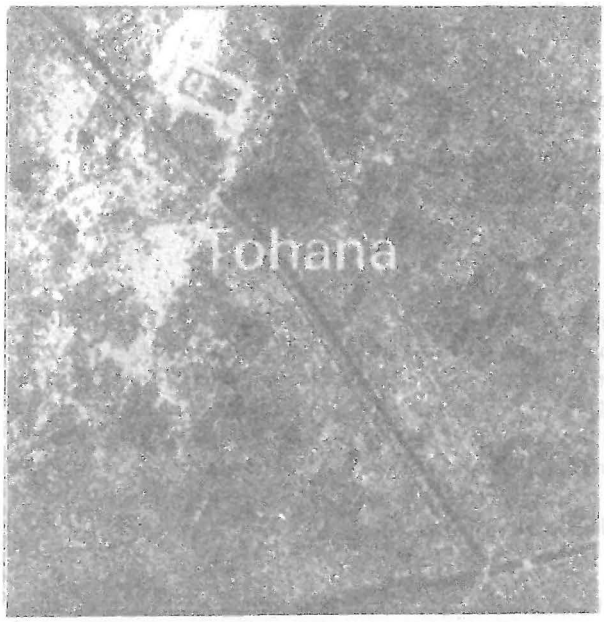

Figure-5a. Urban settlement and related feature as depicted on Radarsat-SAR image of Narwana town

Figure-5b. Corresponding IRS-1C PAN image of Narwana town

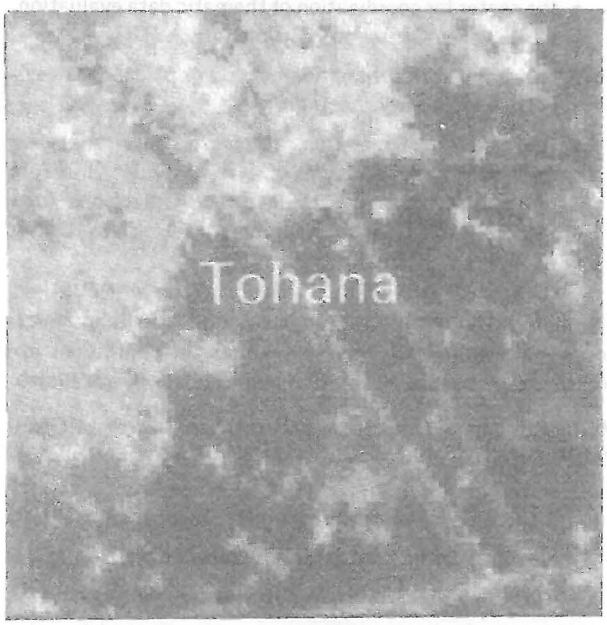

Figure-5c. IRS-1C LISS-III (red band) image of Narwana town